

***Ab initio* study of ferroelectricity in BaTiO<sub>3</sub> nanowires**

G. Pilania, S. P. Alpay, and R. Ramprasad\*

*Chemical, Materials, and Biomolecular Engineering, Institute of Materials Science, University of Connecticut, Storrs, Connecticut 06269, USA*

(Received 15 January 2009; revised manuscript received 19 May 2009; published 24 July 2009)

We present a density-functional theory study of finite-size effects in stoichiometric and nonstoichiometric BaTiO<sub>3</sub> nanowires of varying cross-sectional sizes and sidewall terminations. The tendencies for axial, transverse, and toroidal ferroelectric polarization instabilities in these nanowires have been characterized and possible driving forces underlying these behaviors have been identified. The critical size for ferroelectricity via polarization along the nanowire axis is determined to be 12 Å, regardless of the stoichiometry or nanowire sidewall terminations. The sidewall terminations alter the manner in which axial polarization manifests; for instance, in nonstoichiometric BaO-terminated nanowires, a “core-shell-type” polarization results beyond the critical size, while in all other cases, roughly uniform polarization along the same direction was observed across the entire cross section. A tendency for transverse polarization (i.e., normal to the nanowire axis) occurs in nanowires with a cross-sectional size of 16 Å displaying TiO<sub>2</sub>-terminated sidewall facets. This tendency is accompanied by a toroidal or vortex polarization state, with the toroidal moment along the nanowire axis, to mitigate the depolarizing fields due to transverse polarization.

DOI: [10.1103/PhysRevB.80.014113](https://doi.org/10.1103/PhysRevB.80.014113)

PACS number(s): 77.80.-e, 77.22.Ej, 77.84.Dy

**I. INTRODUCTION**

Owing to their potentially high dielectric constant and their ability to support switchable polarization states, ferroelectric nanoparticles (NPs) and nanowires (NWs) are being considered as fillers in flexible capacitor organic films<sup>1</sup> and as media for next-generation ultrahigh-density computer memories.<sup>2–4</sup> Intense experimental efforts targeted both toward the synthesis of ferroelectric nanostructures with size and shape control,<sup>5–9</sup> as well as characterization of their physical, dielectric, and polarization states with unprecedented precision are underway.<sup>10–13</sup> For instance, advanced probing techniques such as piezoresponse force microscopy (PFM) (Ref. 10) and ultrahigh vacuum scanning probe microscopy (SPM) (Ref. 11) have pushed the resolution limit of a local domain structure to less than 100 Å. Using these techniques, it has been shown that stable polarization states in individual single-crystalline barium titanate (BTO) NWs can be reproducibly induced, sensed, and manipulated along both the axial<sup>12</sup> and transverse<sup>13</sup> directions of the NW.

Paralleling and complementing the above developments is a growing number of theoretical efforts. The past decade has seen a revolution in the theoretical understanding of ferroelectricity through first-principles density-functional-theory-based (DFT-based) methods, first-principles-derived effective Hamiltonian techniques, and the Landau-Ginzburg-Devonshire-theory-based phenomenological approaches.<sup>14</sup> First-principles DFT methods, owing to their computational complexity, have largely been used to study bulk and thin-film geometries of ferroelectric systems, typically, containing a few to several tens of atoms per repeating unit cell.<sup>15</sup> These “typical” numbers are increasing rapidly allowing for studies of ferroelectric nanostructures; for instance, recent investigations (the only first-principles studies of ferroelectric NWs to date) indicate that the critical size for the onset of ferroelectricity along the NW axis is about 12 Å in stoichiometric BTO NWs (Ref. 16) and about 16 Å in nonstoichiometric

TiO<sub>2</sub>-terminated PbTiO<sub>3</sub> NWs.<sup>17</sup> To circumvent the practical limitations imposed by fully first-principles techniques, parameterized effective Hamiltonian<sup>18–20</sup> and phenomenological approaches<sup>21</sup> that permit studies of ferroelectric systems with effectively several thousand atoms have been used. Although not as accurate or versatile as fully first-principles approaches (due to their inability to explicitly treat atoms, surface terminations, and chemical environments), these efforts have been instrumental at predicting the existence of exotic polarization states such as the toroidal, or vortex, states in ferroelectric nanodisks as small as 28 Å and multiple vortices in nanodisks larger than 300 Å.<sup>19–21</sup> Still, a satisfactory understanding of the *atomic*-level origins and mechanisms that result in dielectric response, diverse polarization states, and the dependence of these states on size and surface chemistry down to the nanometer regime is unavailable at the present time.

Here, we present a fully *ab initio* DFT investigation of polarization ordering in ultrathin free-standing BTO [001] NWs whose bulk unit cell is shown in Fig. 1(a). A comprehensive characterization of the dependence of the polarization states on the size of the NW and the type of the NW sidewall surface termination has been performed. Among the exciting findings of this work are (1) the presence of axial polarization in NWs as thin as 12 Å regardless of NW stoichiometry and sidewall terminations, (2) the complex dependence of the manner of axial polarization on the NW sidewall terminations, (3) the stabilization of an off-axis transverse polarization component in NWs of size 16 Å, and (4) the preponderance of a vortex polarization state to mitigate the depolarizing fields due to the transverse polarization.

This paper is organized as follows. Details concerning the NW structures, including geometry, stoichiometry, and surface terminations are provided in Sec. II. The procedure adopted to quantify the tendency for polarization distortions is prescribed in Sec. III. Details pertaining to the specific computational approach, approximations used, and geometry constraints imposed are discussed in Sec. IV. Results are pre-

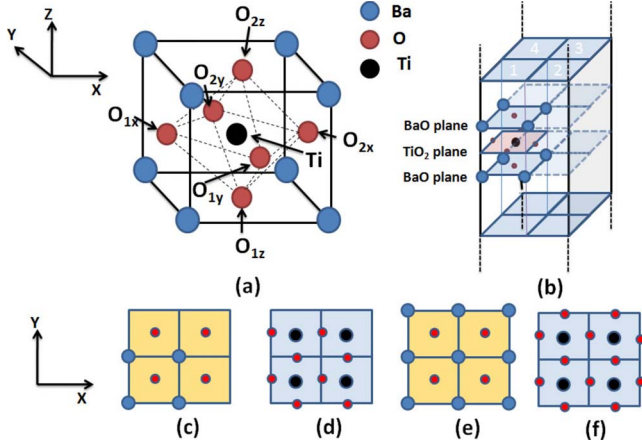


FIG. 1. (Color online) (a) BTO unit cell showing the  $\text{TiO}_6$  octahedron and atom labels used in the definition of polarization distortions (see text for details). (b) A  $2 \times 2$  nanowire showing alternate stacking of BaO and  $\text{TiO}_2$  planes along the NW axis. [(c) and (d)] Transverse view (along  $x$ - $y$  plane) of successive BaO and  $\text{TiO}_2$  planes, respectively, in a stoichiometric  $2 \times 2$  ( $S$ - $2 \times 2$ ) NW. [(e) and (f)] Transverse view (along  $x$ - $y$  plane) of successive BaO and  $\text{TiO}_2$  planes, respectively, in a BaO-terminated nonstoichiometric  $2 \times 2$  ( $\text{BaO}$ - $2 \times 2$ ) NW.

sented in Sec. V in two parts; stoichiometric NWs were used to perform density-of-states (DOS) analysis and to determine the energetic driving forces for polarization instabilities along the NW axis (Sec. V A), and nonstoichiometric NWs allowed for a study of off-axis polarization instabilities (Sec. V B). In Sec. VI, we comment about the possible mechanisms that favor spontaneous off-axis polarizations in BTO NWs. Finally, we summarize conclusions in Sec. VI.

## II. DETAILS OF NW STRUCTURES

Both stoichiometric and nonstoichiometric infinite BTO NWs were considered in this study. Stoichiometric NWs contained an integral number of BTO units (each with 1 Ba, 1 Ti and, 3 O atoms) with the BTO units arranged in a  $n \times n$  square grid along the plane normal to the NW axis. These are henceforth referred to as  $S$ - $n \times n$  NWs. Infinite repetitions of the BTO units along the NW axis resulted in alternate stacking of BaO and  $\text{TiO}_2$  planes [Fig. 1(b)] and, consequently, in  $n^2$  infinite -O-Ti-O- chains along the NW axis. Owing to the stoichiometry, two of the NW sidewall facets are BaO terminated and the other two are  $\text{TiO}_2$  terminated. Figures 1(c) and 1(d) show alternate BaO and  $\text{TiO}_2$  planes normal to the axis of a  $S$ - $2 \times 2$  NW.

Although stoichiometric NWs allow for an unambiguous definition of energies per BTO unit (e.g., total energy, ferroelectric well depth, etc.), the inherent asymmetry of these structures results in a polarization component normal to the NW axis. This asymmetry can prevent a clear understanding of the intrinsic tendency of the system to adopt certain polarization configurations. Moreover, real NWs will display facets that are either all BaO or all  $\text{TiO}_2$  terminated, depending on which of the two surface facets is stabilized in a given chemical environment. Owing to these factors, we have also

considered a set of BaO- and  $\text{TiO}_2$ -terminated nonstoichiometric NWs henceforth referred to as  $\text{BaO}$ - $n \times n$  and  $\text{TiO}_2$ - $n \times n$  NWs, respectively.  $\text{BaO}$ - $n \times n$  ( $\text{TiO}_2$ - $n \times n$ ) NWs were created by adding BaO ( $\text{TiO}_2$ ) layers to the  $\text{TiO}_2$  (BaO) facets of  $S$ - $n \times n$  NWs. Figures 1(e) and 1(f) show alternate BaO and a  $\text{TiO}_2$  planes normal to the axis of a  $\text{BaO}$ - $2 \times 2$  NW.

## III. LOCAL FERROELECTRIC DISTORTIONS

The off-center displacements of Ti atoms, which, in the reference paraelectric state, are at the centers of O octahedra, were used as a quantitative measure of the *local* ferroelectric distortions. The BTO unit cell of Fig. 1(a) also shows the O octahedron. The displacement of the central Ti atom can be represented by a vector  $\mathbf{d}$  with  $d^x$ ,  $d^y$ , and  $d^z$  being its  $x$ ,  $y$ , and  $z$  components, respectively. Each of these components can further be defined in terms of the locations of the Ti and the six neighboring O atoms [Fig. 1(a)], as follows:

$$\begin{aligned} d^x &= x_{\text{O}_{1x}} + x_{\text{O}_{2x}} - 2x_{\text{Ti}}, \\ d^y &= y_{\text{O}_{1y}} + y_{\text{O}_{2y}} - 2y_{\text{Ti}}, \\ d^z &= z_{\text{O}_{1z}} + z_{\text{O}_{2z}} - 2z_{\text{Ti}}, \end{aligned} \quad (1)$$

where  $x_{\text{O}_{1x}}$  represents the  $x$  coordinate of atom  $\text{O}_{1x}$ , etc. The above definition of  $\mathbf{d}$  has been used to quantify the tendency for variation in polarization with position (from one unit cell to the other).

## IV. DETAILS OF THEORETICAL METHODS

All DFT calculations presented here are for 0 K situations and were performed using a numerical atomic-orbital method<sup>22</sup> as implemented in the SIESTA code.<sup>23</sup> The electronic wave functions were expanded using a double-zeta plus polarization basis set, electron-electron interactions were treated within the local-density approximation, and the electron-nuclear interactions were captured using norm-conserving Troullier-Martins pseudopotentials,<sup>24</sup> as has been done before for BTO.<sup>25</sup> With these choices, the properties of the bulk paraelectric (cubic) and the ferroelectric (tetragonal and rhombohedral) phases were reproduced satisfactorily. For instance, the lattice parameter for the cubic phase was computed to be 3.958 Å, the  $a$  and  $c$  lattice parameters for the tetragonal phase to be 3.956 Å and 3.968 Å, respectively, and the lattice parameter and the angle for the rhombohedral phase to be 3.964 Å and 89.99°, all in good agreement with experiments and previous *ab initio* work.<sup>26,27</sup> The tetragonal and rhombohedral phases were 13 and 17 meV lower in energy (per BTO unit), respectively, than the paraelectric cubic phase. The off-center displacement of the Ti atom accompanying ferroelectric distortions in bulk can be represented using  $\mathbf{d}$  as defined above. Needless to say,  $d^x = d^y = d^z = 0$  for the cubic phase. For the bulk tetragonal ferroelectric phase, our computed value of  $d^z$  was 0.20 Å (with  $d^x = d^y = 0$ ), in good agreement with prior *ab initio* work and experiments.<sup>26</sup> For the rhombohedral phase, we found

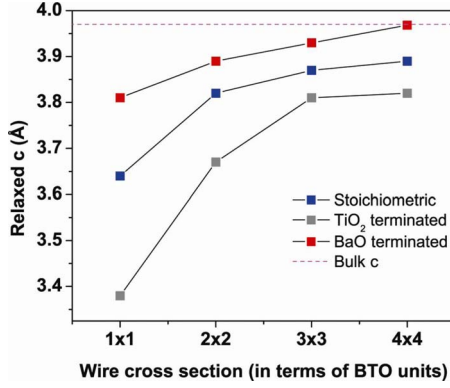


FIG. 2. (Color online) Evolution of equilibrium lattice constant  $c$  as a function of wire cross section for stoichiometric and nonstoichiometric NWs (having either BaO and TiO<sub>2</sub> termination). Corresponding bulk tetragonal value is represented as a horizontal dashed line.

that  $d^x = d^y = d^z = 0.16$  Å, again in good agreement with prior work.<sup>27</sup>

$S-n \times n$ , BaO- $n \times n$ , and TiO<sub>2</sub>- $n \times n$  NW calculations, with  $n=1-4$ , were performed using the supercell method with the NW axis oriented along the tetragonal  $c$  axis (taken here to be along the  $z$  direction) and with the NWs separated by at least 12 Å from the neighboring images normal to the NW axis. [It is worth mentioning that the supercell vectors were chosen to be orthogonal, thereby allowing (disallowing) tetragonal (rhombohedral) ferroelectric distortions. This decision was motivated by the reasoning that a polarization component normal to the NW axis, required by rhombohedral distortions, will lead to energetically unfavorable depolarizing fields. Nevertheless, we will see that, under appropriate conditions, the system is able to find a way to circumvent this constraint.] A set of six special  $k$ -points and atomic forces smaller than 0.02 eV/Å were required to ensure converged results.

## V. RESULTS

For each NW, two cases were considered: (1) Ti atoms constrained to be at the midpoint between the O atoms above

and below (our reference “paraelectric” state with net zero axial polarization, i.e., with  $d^z=0$ ; note, however, that these structures may have a nonzero  $d^x$  or  $d^y$  value depending on the location, stoichiometry, and surface termination) and (2) Ti atoms intentionally displaced from this central position (followed by geometry optimization) in order to determine the tendency for each system to display ferroelectric instability. For each of these two cases, the value of the  $c$  parameter (periodic distance along the NW axis) was optimized. The value of the  $c$  parameter corresponding to the most stable NW for each size and stoichiometry is displayed in Fig. 2 with the horizontal dashed line representing the corresponding value for bulk BTO. Smaller  $c$  values for NWs with smaller cross sections is a consequence of the atoms (most of which are at or close to the sidewall facets) desiring to increase their reduced coordination. The  $c$  value of all NWs asymptotically approach the bulk BTO value. The BaO- $n \times n$  NWs appear to achieve this the quickest and the TiO<sub>2</sub>- $n \times n$  the slowest, with the stoichiometric variety being intermediate. Table I lists the average lateral lattice parameter ( $\bar{a}$ ),  $c$ , and  $c/\bar{a}$  for each of the nonstoichiometric nanowires. The  $c/\bar{a}$  ratio is a measure of tetragonality with larger values of this ratio correlating with an increased tendency for ferroelectric distortions. In fact, the  $c/a$  ratio is equal to 1 and 1.003, respectively, in bulk paraelectric and bulk ferroelectric BTO. For the nonstoichiometric NWs considered here, we see from Table I that the  $c/\bar{a}$  ratio increases with NW size indicating an increased tendency for ferroelectricity with size. This trend is qualitatively similar to that seen in a recent study of PbTiO<sub>3</sub> NWs (Ref. 17) and is consistent with the onset of ferroelectricity at a critical size as will be discussed shortly. It is worth noting that the actual value of the  $c/\bar{a}$  ratio that signifies the onset of ferroelectricity need not be 1 in the case of NWs (as opposed to bulk) due to the presence of coordinative unsaturations in the NW surface facets.

### A. Stoichiometric NWs

First, we discuss the polarization behavior of stoichiometric NWs. Their tendency for ferroelectric distortion was quantified in terms of the “ferroelectric well depth,” defined as the energy difference (per BTO unit) between the refer-

TABLE I. Averaged lateral lattice parameters ( $\bar{a}$ ), the  $c$  lattice parameter, and the  $c/\bar{a}$  ratios of PbO and TiO<sub>2</sub> terminated nanowires as a function of cross-sectional size.

Nanowire size	1 × 1	2 × 2	3 × 3	4 × 4	Bulk
		BaO terminated			
$\bar{a}$	3.70	3.78	3.81	3.83	3.96
$c$	3.64	3.82	3.87	3.89	3.97
$c/\bar{a}$	0.984	1.011	1.016	1.016	1.003
		TiO <sub>2</sub> terminated			
$\bar{a}$	3.74	3.84	3.85	3.88	3.96
$c$	3.38	3.67	3.81	3.82	3.97
$c/\bar{a}$	0.904	0.956	0.990	0.985	1.003

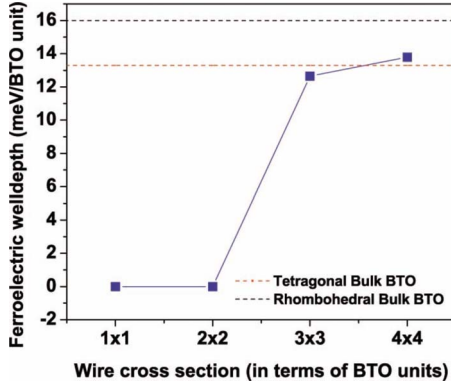


FIG. 3. (Color online) Ferroelectric well depth (defined as the energy difference between the paraelectric and ferroelectric phases) per BTO unit for stoichiometric NWs as a function of wire cross section. Corresponding bulk values for tetragonal and rhombohedral phases are shown as horizontal dashed lines.

ence paraelectric structure with  $d^z=0$  and the distorted ferroelectric structure (should this be stable). In the case of the S-1  $\times$  1 and S-2  $\times$  2 NWs, the only stable structures were the paraelectric ones. In contrast, the ferroelectric states were stable in S-3  $\times$  3 and S-4  $\times$  4 NWs with ferroelectric well depths of 12.8 and 13.8 meV/BTO unit, respectively, close to the corresponding value for bulk tetragonal BTO but smaller than for bulk rhombohedral BTO, as shown in Fig. 3. The off-center positions along the  $z$  direction of Ti atoms were used to determine  $d^z$  for all Ti atoms, which are plotted in Fig. 4 for both S-3  $\times$  3 and S-4  $\times$  4 NWs. It can be seen that the magnitude of the ferroelectric distortions are, in general, smaller than in bulk BTO and that the distortions are much larger at and close to TiO<sub>2</sub>-terminated facets than at and close to BaO-terminated facets (similar to behaviors seen in BTO slabs).<sup>26</sup> From these results, and Fig. 3, it can be concluded that the ferroelectric distortion is stabilized over the paraelectric state even in NWs as small as 12 Å, in agreement with prior *ab initio* work.<sup>16</sup>

In order to better understand the circumstances that render the ferroelectric state more stable, we carried out decomposed DOS analysis, in which the contribution to the total DOS due to each BTO unit of the NW is identified. The decomposed unit DOS are depicted in Fig. 5 for the S-3  $\times$  3 NW. Eight of the nine BTO units lie along either the BaO- or TiO<sub>2</sub>-terminated facets and unit 5 is completely sur-

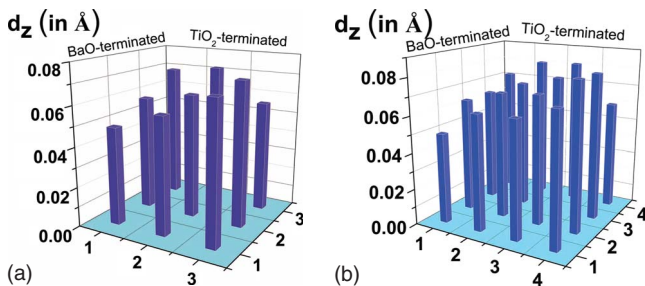


FIG. 4. (Color online) Axial polarization distortion (characterized in terms of  $d^z$ ) for (a) S-3  $\times$  3 and (b) S-4  $\times$  4 nanowires.  $x$  and  $y$  labels index the unit cells across the nanowire cross section.

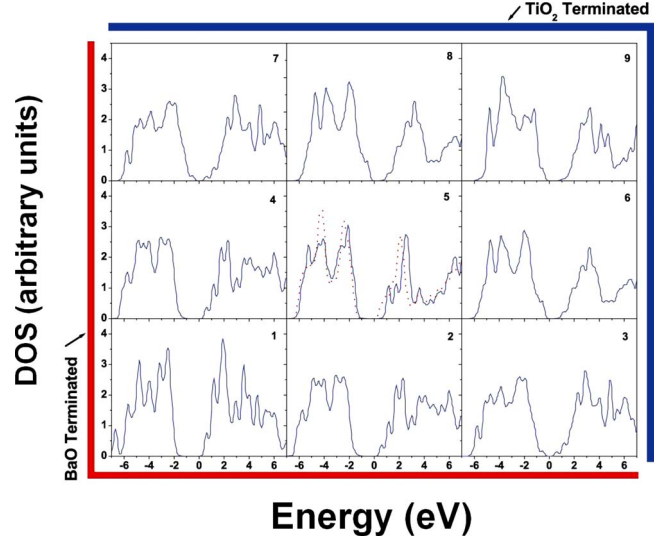


FIG. 5. (Color online) Decomposed density of states in terms of individual BTO units for S-3  $\times$  3 BTO NW. Dotted line in panel 5 represents DOS for a bulk BTO unit.

rounded by the other BTO units. But for the fact that the band gap corresponding to unit 5 is larger than the bulk BTO band gap (due to quantum confinement), its DOS is identical to that of bulk BTO, as can be seen in Fig. 5. The DOS of units lining the TiO<sub>2</sub>- and BaO-terminated facets display, respectively, significant and modest narrowing of the band gap, relative to unit 5, due to additional (surface) states created in the band gap, reminiscent of the behavior displayed by BTO slabs.<sup>26</sup> The largest narrowing of the band gap is seen in units 3 and 7 containing both TiO<sub>2</sub>- and BaO-terminated facets. These results indicate that the presence of at least one BTO unit completely surrounded by a “shell” of other BTO units is accompanied by the onset of ferroelectricity.

### B. Nonstoichiometric NWs

Next, we turn our attention to the nonstoichiometric BaO- $n \times n$  and TiO<sub>2</sub>- $n \times n$  NWs. Here, in addition to the axial ferroelectric distortion, quantified in terms of  $d^z \hat{z}$ , we also consider the transverse component of the distortion (i.e., along a plane normal to the NW axis), defined as  $\mathbf{d}^\perp = d^x \hat{x} + d^y \hat{y}$ . Among the BaO- $n \times n$  NWs, axial polarization was not stable in the BaO-1  $\times$  1 and BaO-2  $\times$  2 NWs, similar to the stoichiometric case. Hence, we focus only on BaO-3  $\times$  3 and BaO-4  $\times$  4 NWs, whose  $d^z$  and  $\mathbf{d}^\perp$  are shown in Fig. 6. It is clear that axial polarization is realized only in the core of the NWs [Figs. 6(a) and 6(b)], i.e., in those BTO units completely surrounded by at least one BTO shell. It is worth noting that in the outer “shell” region, although the  $d^z$  value is quite small, its sign is opposite that of  $d^z$  in the core region. It can thus be concluded that BTO NWs bound by BaO facets will display core-shell polarization, as has been proposed earlier based on PFM measurements.<sup>10</sup> In the core region, the level of the distortion, i.e.,  $d^z$  value, is closer to the corresponding bulk tetragonal value of 0.20 Å than displayed by stoichiometric NWs. Figures 6(c) and 6(d) display  $\mathbf{d}^\perp$  for the BaO-3  $\times$  3 and BaO-4  $\times$  4 NWs. Although the Ti

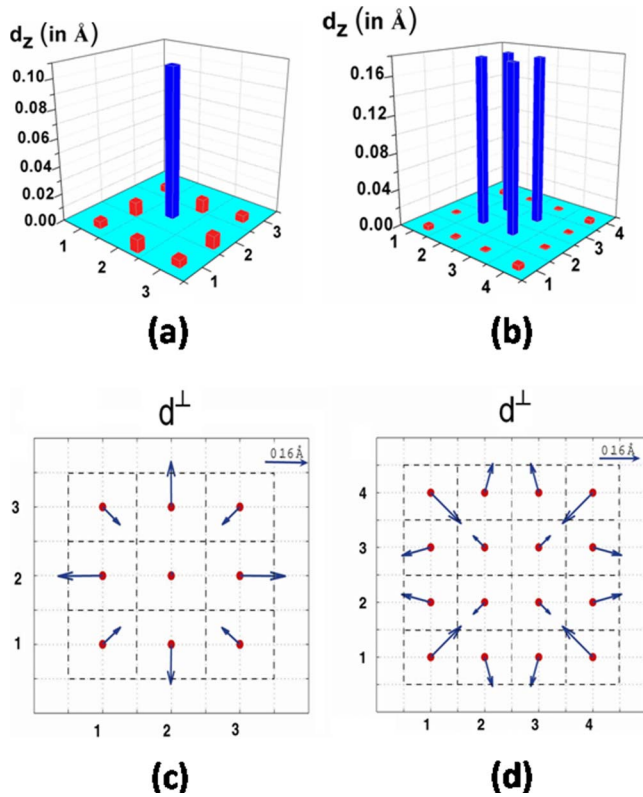


FIG. 6. (Color online) [(a) and (b)] Calculated axial polarization distortion (characterized in terms of  $d^z$ ) for BaO- $3 \times 3$  and BaO- $4 \times 4$  NWs, respectively. Blue and red histograms represent positive and negative values of  $d^z$ . [(c) and (d)] Calculated transverse polarization patterns (characterized in terms of  $\mathbf{d}^\perp$ ) for BaO- $3 \times 3$  and BaO- $4 \times 4$  NWs, respectively.  $x$  and  $y$  labels index the unit cells across the nanowire cross section.

atoms do not display a tendency to all move radially inward or outward, the fourfold symmetry of the NW cross section is reflected in the transverse distortions. The clear tendency for radial polarization is largely driven by relaxation and reconstruction at surface facets, which tend to diminish as the center of the NW is approached. None of these NWs display a net dipole moment along any of the transverse directions.

The  $\text{TiO}_2$ - $1 \times 1$  and  $\text{TiO}_2$ - $2 \times 2$  NWs having size below the critical size of ferroelectricity bear no spontaneous polarization. *It thus appears that the critical size for ferroelectricity in BTO NWs (with polarization along the NW axis) is about 12 Å, regardless of stoichiometry or surface terminations.* Figure 7 shows the axial and the transverse components of the ferroelectric distortions for the  $\text{TiO}_2$ - $3 \times 3$  and  $\text{TiO}_2$ - $4 \times 4$  NWs, which show qualitatively different tendencies compared to the BaO-terminated NWs. The axial component is significant in both these  $\text{TiO}_2$ -terminated NWs regardless of the location of the Ti atom (although  $d^z$  corresponding to corner and core Ti atoms are somewhat reduced compared to that of the others). The core-shell behavior seen in the BaO-terminated NWs is not displayed here. Focusing next on the transverse component of the distortion, it can be seen that all Ti atoms tend to move radially inward significantly rather than the “mixed” trend shown by

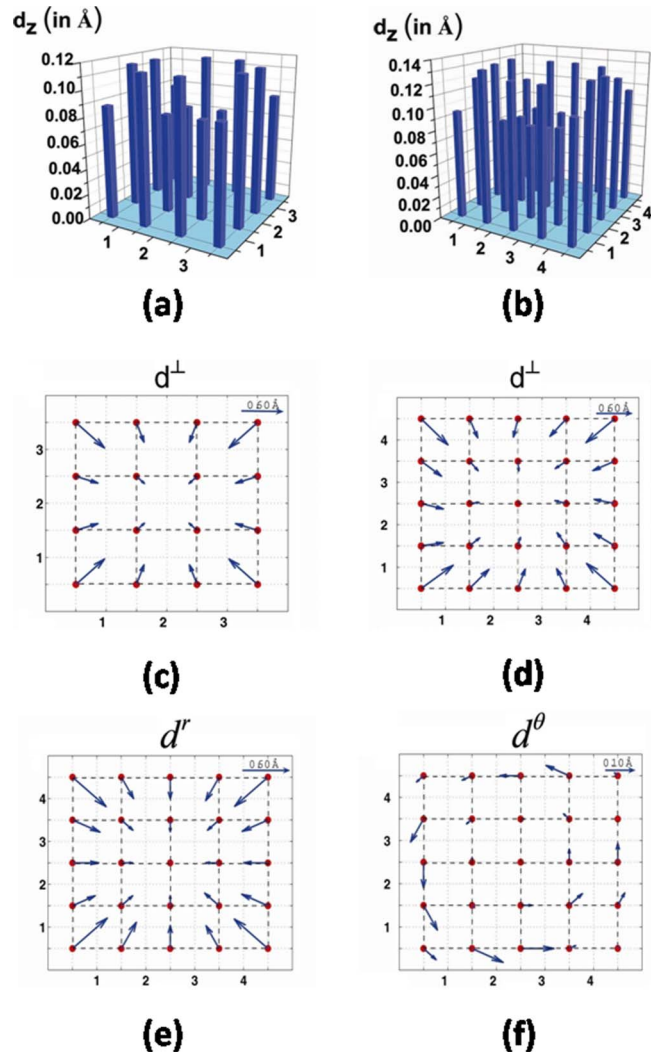


FIG. 7. (Color online) [(a) and (b)] Axial polarization distortion in  $\text{TiO}_2$ - $3 \times 3$  and  $\text{TiO}_2$ - $4 \times 4$  NWs, respectively. [(c) and (d)] Transverse polarization patterns of  $\text{TiO}_2$ - $3 \times 3$  and  $\text{TiO}_2$ - $4 \times 4$  NWs, respectively. [(e) and (f)] Radial and azimuthal decompositions, respectively, of the transverse polarization pattern of the  $\text{TiO}_2$ - $4 \times 4$  NW shown in (d).  $x$  and  $y$  labels index the Ti atoms across the nanowire cross section.

BaO- $n \times n$  NWs. Nevertheless, the important impact of the  $\text{TiO}_2$  termination is that the surface Ti atoms are exposed and no longer contained within the  $\text{TiO}_6$  octahedra. Hence, they experience more significant inward relaxations (to compensate for their coordinative unsaturations) than the near-surface Ti atoms in BaO-terminated NWs. That the surface termination is crucial in determining the tendency for the type of ferroelectric distortion can be seen by comparing the results for the BaO- $4 \times 4$  and  $\text{TiO}_2$ - $3 \times 3$  NWs, as both these NWs have 16 -O-Ti-O- chains along the NW axis.

The most remarkable polarization behavior is displayed by the  $\text{TiO}_2$ - $4 \times 4$  NW, whose transverse polarization distortions are depicted in Fig. 7(d). This NW contains 25 -O-Ti-O- chains along its axis, the most number of chains among NWs considered here. Although  $\mathbf{d}^\perp$  for the  $\text{TiO}_2$ - $4 \times 4$  NW looks qualitatively similar to that for the  $\text{TiO}_2$ - $3 \times 3$  case, a more careful inspection indicates that the trans-

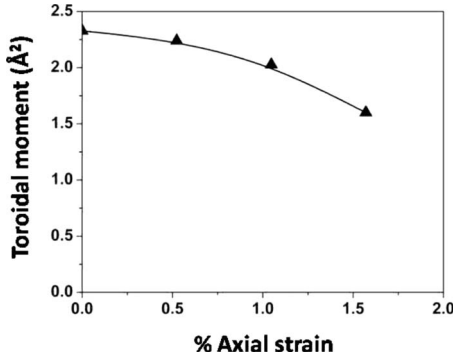


FIG. 8. Effect of axial strain on toroidal moment for the  $\text{TiO}_2\text{-}4 \times 4$  NW.

verse polarization distortions in the  $\text{TiO}_2\text{-}4 \times 4$  NW are not entirely radial (cf. Figs. 7(c) and 7(d)). The  $\text{TiO}_2\text{-}4 \times 4$  NW  $\mathbf{d}^\perp$  were further decomposed into radial and azimuthal components (i.e.,  $\mathbf{d}^\perp = d^r \hat{r} + d^\theta \hat{\theta}$ ), which are shown in Figs. 7(e) and 7(f). Strikingly, the azimuthal distortion is reminiscent of the vortex polarization state anticipated in ferroelectric nanostructures based on recent effective Hamiltonian simulations.<sup>19,20</sup> Although the azimuthal distortions are an order of magnitude smaller than the corresponding radial distortions, they are comparable in magnitude to the axial distortions. The lack of complete fourfold symmetry of  $d^\theta$  results in a net dipole moment of  $0.06\hat{x} - 0.03\hat{y}$  in atomic units. Several attempts were made to stabilize a  $\text{TiO}_2\text{-}4 \times 4$  NW with no net off-axis dipole moment, but all such attempts converged toward structures with a nonzero dipole moment, reflecting this system's tendency to stay transversely polarized. *These results thus indicate that the critical size for the occurrence of a transverse polarization instability in BTO NWs is about 16 Å (at 0 K).* We make the observation that our results are consistent with recent experimental work. For instance, SPM investigations by Yun *et al.*<sup>11</sup> have shown that an off-axis component of polarization can be easily induced and retained over a long period of time in single-crystal BTO NWs. Carrying the work further, Spanier *et al.*<sup>13</sup> established that the critical size for stable transverse off-axis polarization at room temperature to be 30 Å which when extrapolated to low temperature indicate a critical size of  $\sim 8$  Å.

To study the effect of axial strain on the vortex polarization state in the  $\text{TiO}_2\text{-}4 \times 4$  NW, calculations were carried out by constraining the  $c$  lattice parameter fixed at different values (viz., 3.84, 3.86, and 3.88 Å) while all the internal degrees of freedom in the supercell were allowed to relax. We define an axial toroidal moment as follows:

$$\tau_z = \sum_i d_i^\theta \times R_i, \quad (2)$$

where  $R_i$  denotes the position vector of  $i$ th Ti atom in the wire cross section with respect to the center of the wire,  $d_i^\theta$  is the contribution of  $i$ th Ti atom to the azimuthal component of polarization [as plotted in Fig. 7(f)] and the sum runs over all Ti atoms in the wire cross section. In Fig. 8 we plot  $\tau_z$  as a function of axial strain for the  $\text{TiO}_2\text{-}4 \times 4$  NW. Our results

clearly show that application of axial tensile strain destabilizes the vortex state in the NW.

## VI. DISCUSSION

Finally, we comment about the possible driving forces underlying the tendency of BTO NWs to exist in a vortex state with a net transverse dipole moment. As mentioned above, *ab initio* derived effective Hamiltonian treatments have identified such a vortex polarization tendency in ferroelectric nanodisks (this behavior is a natural conceptual extension foreseen decades earlier in the case of ferromagnetic nanostructures by Kittel<sup>28</sup>). In the case of nanodisks, the geometry of the system favors polarization along the nanodisk surface (as polarization along the disk axis will lead to unfavorably large depolarizing fields). Still, as the system size decreases, the depolarizing fields along the nanodisk surface can become significant. In order to satisfy both the need of the system to stay polarized (the intrinsic tendency of ferroelectrics) and minimize depolarizing fields, the nanodisk system could adopt a vortex state in which depolarizing fields are eliminated due to closed polarization loops. The resultant vortex polarization distribution is thus a direct consequence of energy minimization in the presence of polarization fields, dipole-dipole interactions, and electrical and geometric boundary conditions.

However, we do not anticipate a vortex state in the case of infinite NWs. Here, the system can satisfy its need to stay polarized by adopting an axial polarization (the preferred polarization direction dictated by geometry). Net transverse components of the polarization (and vortex states to mitigate the accompanying depolarizing fields) are not expected. Nevertheless, we do see this behavior in the case of the  $\text{TiO}_2\text{-}4 \times 4$  BTO NW considered here. We believe that this tendency may, in part, be due to the nature of bulk BTO to adopt a rhombohedral structure with polarization along the  $\langle 111 \rangle$  pseudocubic directions (rather than along the  $[001]$  axis of the NW). Thus, since the NW axis is forced to be along the  $[001]$  direction, the system displays a tendency to be polarized along an off-axis direction in NWs larger than a certain critical size. The vortex state occurs to minimize the effect due to the depolarizing fields. Extensions to the current calculations, both in terms of larger NW cross-sectional sizes as well as in the form of studies of systems other than BTO, are required to obtain a better understanding of the intricate and general factors that contribute to polarization in ferroelectric nanostructures.

## VII. SUMMARY

We have performed a DFT study of free-standing infinite BTO  $[001]$  nanowires. Both stoichiometric and nonstoichiometric nanowires were considered, with the former containing both BaO and  $\text{TiO}_2$  sidewall facets and the latter bound by either BaO or  $\text{TiO}_2$  sidewall facets. Our calculations indicate that regardless of stoichiometry or sidewall termination, the critical size for the onset of ferroelectricity with polarization along the nanowire axis is about 12 Å at 0 K. The degree of polarization (quantified in terms of off-center

Ti atom displacements in  $\text{TiO}_6$  octahedra) and the energetic driving force for the ferroelectric instability (quantified in terms of the ferroelectric well depth) are comparable to those of bulk BTO even in ultrathin nanowires. In the case of  $\text{TiO}_2$ -terminated symmetric nonstoichiometric nanowires with a size of about 16 Å, a polarization instability along a transverse direction, accompanied by a vortex polarization state, was also observed using DFT computations. While further work is required to better understand the polarization tendencies of ferroelectric materials with reduced dimensionality, accurate atomic-level investigations of such systems

using fully *ab initio* computations is increasingly becoming possible.

#### ACKNOWLEDGMENTS

G.P. and R.R. acknowledge financial support of this work by a grant from the Office of Naval Research, and computational support from a National Science Foundation Teragrid Resource Allocation. The authors would also like to acknowledge stimulating discussions with Steve Boggs.

\*rampi@ims.uconn.edu

- <sup>1</sup>V. Tomer and C. A. Randall, J. Appl. Phys. **104**, 074106 (2008).
- <sup>2</sup>J. F. Scott, Science **315**, 954 (2007).
- <sup>3</sup>P. R. Evans, X. Zhu, P. Baxter, M. McMillen, J. McPhillips, F. D. Morrison, J. F. Scott, R. J. Pollard, R. M. Bowman, and J. M. Gregg, Nano Lett. **7**, 1134 (2007).
- <sup>4</sup>I. Naumov, L. Bellaiche, and H. Fu, Nature (London) **432**, 737 (2004).
- <sup>5</sup>M. Alexe, D. Hesse, V. Schmidt, S. Senz, H. J. Fan, M. Zacharias, and U. Gösele, Appl. Phys. Lett. **89**, 172907 (2006).
- <sup>6</sup>Y. Luo, I. Szafraniak, N. D. Zakharov, V. Nagarajan, M. Steinhart, R. B. Wehrspohna, J. H. Wendorff, R. Ramesh, and M. Alexeb, Appl. Phys. Lett. **83**, 440 (2003).
- <sup>7</sup>Y. B. Mao, S. Banerjee, and S. S. Wong, J. Am. Chem. Soc. **125**, 15718 (2003).
- <sup>8</sup>J. J. Urban, W. S. Yun, Q. Gu, and H. J. Park, J. Am. Chem. Soc. **124**, 1186 (2002).
- <sup>9</sup>J. Liu, X. Li, and Y. J. Li, J. Nanosci. Nanotechnol. **2**, 617 (2002).
- <sup>10</sup>Z. Wang, A. P. Suryavanshi, and M.-F. Yua, Appl. Phys. Lett. **89**, 082903 (2006).
- <sup>11</sup>W. S. Yun, J. J. Urban, Q. Gu, and H. Park, Nano Lett. **2**, 447 (2002).
- <sup>12</sup>Z. Wang, J. Hu, and M. Yu, Nanotechnology **18**, 235203 (2007).
- <sup>13</sup>J. E. Spanier, A. Kolpak, I. Grinberg, J. J. Urban, L. Ouyang, W. S. Yun, A. M. Rappe, and H. Park, Nano Lett. **6**, 735 (2006).
- <sup>14</sup>*Physics of Ferroelectrics: A Modern Perspective*, edited by K. Rabe, Ch. H. Ahn, and J.-M. Triscone (Springer-Verlag, Berlin, 2007).
- <sup>15</sup>M. Dawber, K. F. Rabe, and J. F. Scott, Rev. Mod. Phys. **77**, 1083 (2005).
- <sup>16</sup>G. Geneste, Appl. Phys. Lett. **88**, 112906 (2006).
- <sup>17</sup>T. Shimada, S. Tomoda, and T. Kitamura, Phys. Rev. B **79**, 024102 (2009).
- <sup>18</sup>W. Zhong, D. Vanderbilt, and K. M. Rabe, Phys. Rev. Lett. **73**, 1861 (1994).
- <sup>19</sup>I. Naumov and A. M. Bratkovsky, Phys. Rev. Lett. **101**, 107601 (2008).
- <sup>20</sup>H. Fu and L. Bellaiche, Phys. Rev. Lett. **91**, 257601 (2003).
- <sup>21</sup>J. Wang, M. Kamlah, T.-Y. Zhang, Y. Li, and L.-Q. Chen, Appl. Phys. Lett. **92**, 162905 (2008).
- <sup>22</sup>R. Martin, *Electronic Structure: Basic Theory and Practical Methods* (Cambridge University Press, New York, 2004).
- <sup>23</sup>J. M. Soler, E. Artacho, J. D. Gale, A. Garcia, J. Junquera, P. Ordejón, and D. J. Sanchez-Portal, J. Phys.: Condens. Matter **14**, 2745 (2002).
- <sup>24</sup>N. Troullier and J. L. Martins, Phys. Rev. B **43**, 1993 (1991).
- <sup>25</sup>J. Junquera, M. Zimmer, P. Ordejón, and Ph. Ghosez, Phys. Rev. B **67**, 155327 (2003).
- <sup>26</sup>J. Padilla and D. Vanderbilt, Phys. Rev. B **56**, 1625 (1997).
- <sup>27</sup>Ph. Ghosez, X. Gonze, and J. P. Michenaud, Ferroelectrics **220**, 1 (1999).
- <sup>28</sup>C. Kittel, Phys. Rev. **70**, 965 (1946).